Appl. Phys. B 77, 681–686 (2003)
DOI: 10.1007/s00340-003-1298-0

Applied Physics B
Lasers and Optics

A. REINHOLDT[1,✉]
R. DETEMPLE[1]
A.L. STEPANOV[1]
T.E. WEIRICH[2]
U. KREIBIG[1]

Novel nanoparticle matter: ZrN-nanoparticles

[1] I. Physikalisches Institut 1A, RWTH Aachen, Postfach, 52056 Aachen, Germany
[2] Gemeinschaftslabor für Elektronenmikroskopie, RWTH Aachen, Ahornstrasse 55, 52074 Aachen, Germany

Received: 9 May 2003/Revised version: 6 August 2003
Published online: 8 October 2003 •

ABSTRACT This work presents the results of the first preparation (to the best of current knowledge) and investigation of ZrN nanoparticles. The particles were produced by laser ablation/evaporation and adiabatic expansion from zirconium nitride powder targets. The particle size could be varied by applying different seeding gas flows. The size distributions were fairly narrow with mean diameters from $\langle 2R\rangle = 5.5$ nm to $\langle 2R\rangle = 6.5$ nm. Compositional analysis by secondary ion mass spectrometry (SIMS) and transmission electron microscopy (TEM) revealed, that almost stoichiometric crystalline particles were formed. The in-situ optical transmission spectroscopy measurements yielded a single plasmon resonance in the visible spectrum.

PACS 81.07.-b; 78.67.-n

1 Introduction

Zirconium nitride bulk material has been subject to extensive investigations, because it exhibits outstanding physical and chemical properties, such as good conductivity, high chemical and thermal stability, hardness, and abrasion resistance. Hence, it is applied to electronic devices and is used for protective and hard coatings [1]. The preparation of ZrN nanoparticles and their investigation, however, has never been reported, as far as current research has determined.

During the transition of bulk material to nanoparticles, some materials undergo dramatic changes in thier electronic and optical properties [2]. One of the consequences in the case of metals is the occurrence of plasmon resonances in the optical spectra, that lead to distinct and narrow absorption bands. Therefore, particle matter formed by many particles, embedded in some matrix or deposited onto some substrate gained attention in the industry and has found applications in practice as base material for optical filters or as pigments for many elemental and compound materials.

The aim of this work is to exam the possibility for the synthesis and to study the basic physical properties of ZrN nanoparticle matter as well as their possible application as color pigments. The first results of these investigations are presented.

✉ Fax: +49 241/80-22331, E-mail: reinholdt@physik.rwth-aachen.de

2 Experimental

For the experiments the laser ablation/evaporation cluster beam apparatus LUCAS was used, which is described in detail by Stepanov et al. [3, 4]. The overview of LUCAS is presented in Fig. 1.

The ZrN target was prepared from 99.5% pure powder (Alfa Aesar, Hf content < 3%). The powder was moistened by a few drops of pure propanol and pressed for about 5 min at a pressure of approximately 2 kbar. The emerging lump was dried in air and put onto the target holder in the source chamber of LUCAS. Subsequently, the apparatus was pumped for several hours and the background pressure dropped to approximately 10^{-8} mbar.

To obtain (almost) stoichiometric ZrN particles during ablation and to avoid their oxidation [5], high purity N_2 seeding gas (99.99990%, Air Products) was applied to the source chamber. The N_2 pressure was up to 1 bar. The target was ablated/evaporated using a Lumonics JK 702H Nd : YAG laser that was operated in pulsed mode with a frequency of 80 Hz and a pulse length of 2 ms. The mean laser power was 290 W and the energy output per pulse was 3.6 J. A collimated particle beam is formed during the adiabatic expansion into the vacuum of the measuring chamber. Usually, the particles were deposited onto silica substrates.

In a special experiment a thick cluster film of 29.4 nm (sample 0) was prepared for secondary ion mass spectrometry (SIMS) analysis of the chemical composition. The particles were deposited onto an ordinary float glass slab fixed by the sample holder in the measuring chamber and covered with a MgF_2 protective top layer (Alfa Aesar, sintered lumps, Ca content 0.1%–1%) by electron beam evaporation. The equivalent film mass thickness d_{XTC} of the deposited material was controlled by a thickness monitor (XTC/2, Leybold/Inficon).

The chemical analysis of the secondary neutral particle fluxes of sample 0 was performed using the secondary ion mass spectrometer VG Microtech SIMS Lab 300 with electron beam post-ionization. During depth profiling, sputter erosion was carried out using a raster scanned Ar^+ ion beam of 3.5 keV primary energy with a current of 700 nA at an angle of 60° (VG EX05 ion gun). The chemical composition was

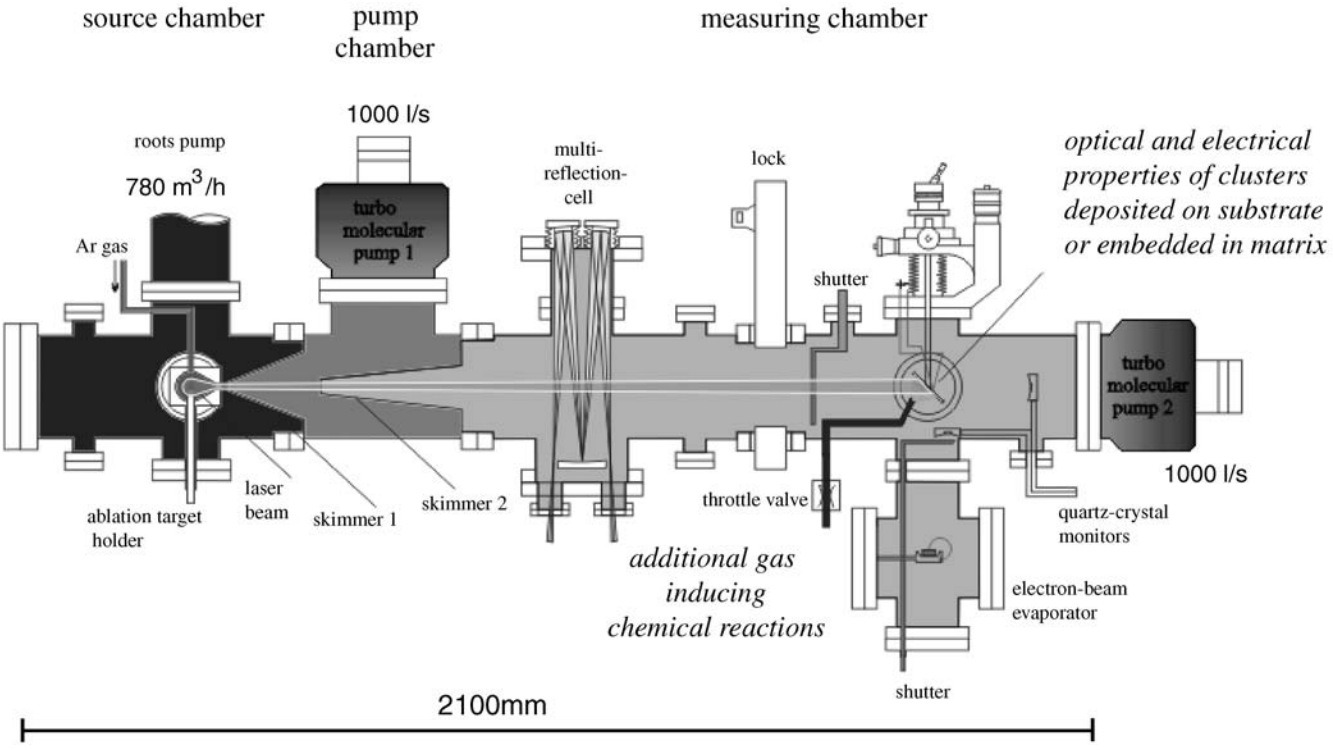

FIGURE 1 The overview of the LUCAS apparatus

Sample	Φ [l/min]	d_{XTC} [nm]
0	1.3	29.4
1	0.6	7.9
2	1.3	10.8
3	2.5	7.5

TABLE 1 Data for the production of the ZrN samples. Φ is the seeding gas flow in the source chamber and d_{XTC} the equivalent film mass thickness of the deposited nanoparticle matter

evaluated using relative sensitivity factors [6], which were obtained from a sputtered ZrN thin film reference sample.

In a second experiment (see Table 1 for preparation data), three ZrN nanoparticle samples, produced with different N_2-seeding gas flows, were deposited onto a silica slab (Herasil 1, Aachener Quarzglas Technologie Heinrich) and onto carbon coated TEM copper grids (samples 1-3). In-situ UV-VIS transmittance spectroscopy was performed with a xenon arc lamp and a MCS 400 multichannel spectrometer (Zeiss).

Subsequently, the samples were taken out of the apparatus and were carried in air to the TEM laboratory. The TEM investigations were done with a FEI TECNAI F20 transmission electron microscope.

3 Results and discussion

3.1 *Sample characterization*

The chemical composition of the ZrN nanoparticles (sample 0) was determined as $Zr_{43}N_{57}$ neglecting the oxygen content (Fig. 2). The relative amount of oxygen concentration could not be quantified due to a missing ZrON calibration sample of known stoichiometry.

TEM brightfield investigations (Figs. 3 and 4) of the samples 1–3 showed that the particles are not perfectly spherical and are densely packed on the carbon film. The images indicate preferential prolate ellipsoidal shapes, which may either have been produced during particle growth, i.e. before deposition, or during deposition by migration and coalescence due to the particle kinetic energy.

In addition the particles are flattened by deformation during the impact on the substrate and by surface tension effects, both causing oblate shapes.

Furthermore, larger coagulation and coalescence aggregates are observed. They may, in part, have been formed already when passing through the expansion nozzle of the source chamber. This could be verified in an additional experi-

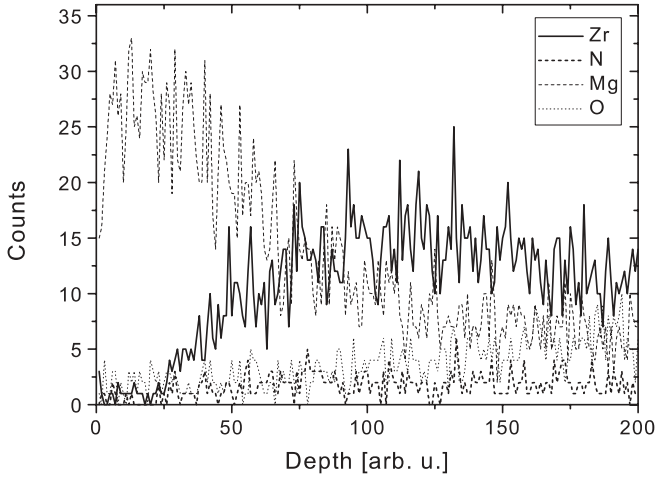

FIGURE 2 SIMS analysis: Detected number of neutrals for the most abundant isotope as a function of the depth from top of the analysed sample. The graph reflects the top coating (MgF_2) and the underlying ZrN nanoparticles. All signals show a statistical noise, which is induced by roughness and by preferential sputtering

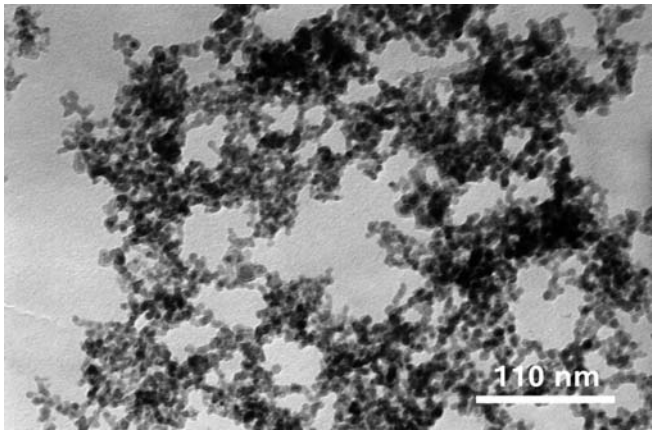

FIGURE 3 Transmission electron micrograph of ZrN particles produced with $\Phi = 2.5\,\mathrm{l/min}$ (sample 3). The particles are densely packed and coagulation can clearly be observed

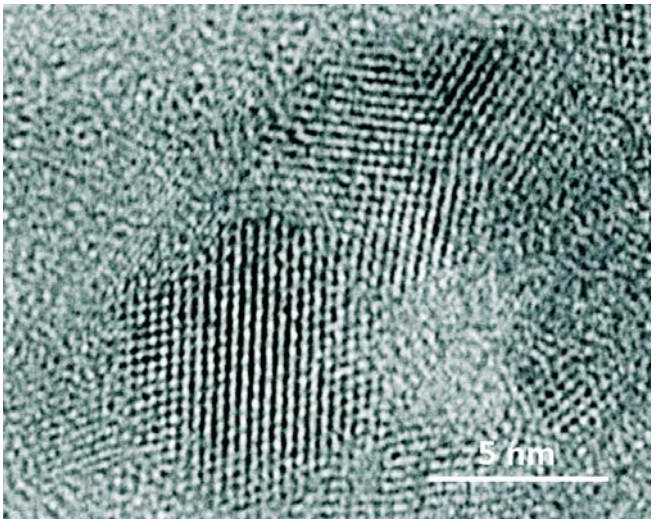

FIGURE 4 High resolution TEM (HRTEM) image of ZrN nanoparticles produced with a seeding gas flow of $\Phi = 0.6\,\mathrm{l/min}$. The particles exhibit round to ellipsoidal shape. Additionally, one can clearly identify the crystalline structure of the particles. The size of the particles is about 5.5 nm (see also Table 2)

ment, where particles were deposited at very low concentrations. Coalesced particles showed up, although the coverage on the substrate was far below one monolayer.

The diffraction pattern (Fig. 5) points clearly to crystalline growth of the particles. The ring pattern analysis combined with energy-filtered TEM measurements revealed, that the samples are composed of zirconium nitride (ZrN, fcc), zirconium monoxide (ZrO, fcc), and zirconium dioxide (ZrO_2, tetragonal). The reflexes of ZrO_2 were much more diffuse than those of ZrN and ZrO and so it is possible to conclude, that ZrO_2 is a decay product which formed as a result of the exposure to air. Due to the relatively sharp rings of the ZrO, it is believed that this species was most likely generated during the preparation by reaction of zirconium with residual oxygen in the plasma plume forming above the target.

In Fig. 6 the particle size distributions are plotted. They were fitted with a log-normal distribution, which considers the asymmetric shapes of the histograms. The results from the analysis are shown in Table 2.

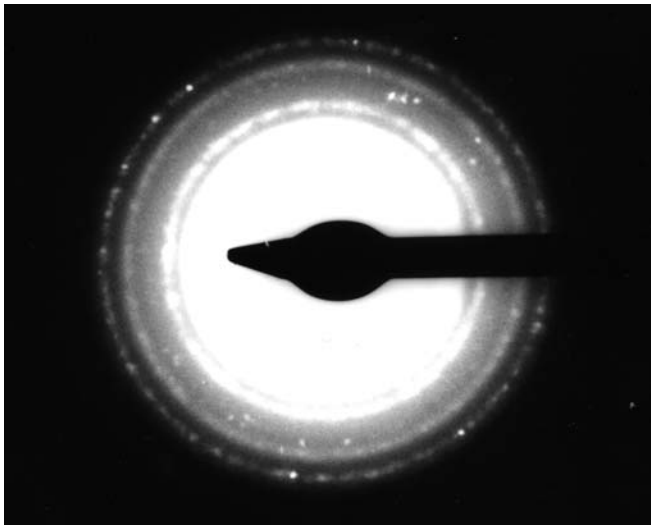

FIGURE 5 Representative diffraction pattern (sample 3)

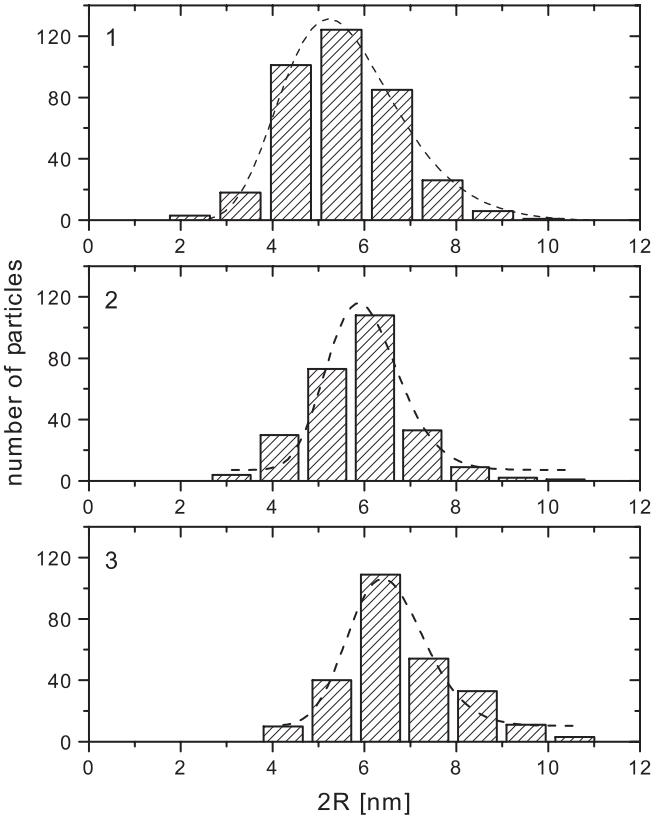

FIGURE 6 Particle size distributions of the samples produced with different N_2 flows of (1) 0.6 l/min, (2) 1.3 l/min, and (3) 2.5 l/min, respectively. R denotes the radius of a nanoparticle. The *dashed curves* are fits with a log-normal distribution

The mean particle diameter is $\langle 2R \rangle = 5.5\,\mathrm{nm}$ for sample 1 and enlarges with increasing seeding gas flow up to $\langle 2R \rangle = 6.5\,\mathrm{nm}$ for sample 3. Hence the average particle volume could be varied by almost a factor of 2. It is suggested that this enlargement is caused by an increased collision rate of atoms in the plasma plume. Thus, a better cooling and faster growth of the nanoparticles is permitted. The widths of the size distributions of all the samples are similar, and are fairly narrow.

Sample	$\langle 2R\rangle$ [nm]	σ [nm]	*Delta* [nm]
1	5.5	1.3	0.1
2	6.0	1.7	0.1
3	6.5	1.3	0.1

TABLE 2 Results of the fit of the particle size distributions shown in Fig. 6. $\langle 2R\rangle$ is the mean diameter of the particles. σ is the standard deviation and $\Delta = \sigma/\sqrt{n}$ is the error of the mean, with n being the particle number. All values are rounded to the first decimal place due to the accuracy of the measurements

3.2 *Optical properties*

Zirconium nitride bulk material is a metal with Drude-like behaviour of the dielectric function [10]. Therefore, small particles should show a plasmon resonance absorption as it is well known for example for Ag and Au [2]. In Fig. 7, classical Mie theory [2] spectra for deposited monodisperse, spherical ZrN nanoparticles with a size of 2, 5, and 10 nm are shown. The calculations were carried out using the dielectric function of thin ZrN films measured by François et al. [10]. To roughly include the influence of the silica-substrate on the optical spectrum, an effective refractive index of

$$n_{\mathrm{M,\,eff}} = \sqrt{\frac{1}{2}\left(\varepsilon_{\mathrm{vac}} + \varepsilon_{\mathrm{silica}}\right)} \approx 1.25$$

was used to model the surrounding [9].

No size effect corrections were performed. A surprising feature of the spectra is, that the plasmon resonance maxima and widths are fixed at $\hbar\omega_{\mathrm{max}}^{\mathrm{calc}} \approx 2.6$ eV and $\Gamma^{\mathrm{calc}} \approx 0.83$ eV for the different particle sizes. That means, that the small changes of the size of the particles do not affect the peak shape in a significant way.

Figure 8 depicts the experimental spectra. The plotted extinction E was derived from the respective measured optical transmission spectra by using the Lambert–Beer law [2, 7]:

$$E(\omega) = \gamma_{\mathrm{e}}(\omega) z = -\ln\left(\frac{I_{\mathrm{t}}(\omega)}{I_0(\omega)}\right).$$

$\gamma_{\mathrm{e}}(\omega)$ is the extinction constant, z the thickness of the nanoparticle layer, $I_{\mathrm{t}}(\omega)$ the intensity of the transmitted and $I_0(\omega)$ the intensity of the incident light.

The optical data of the three samples show pronounced single plasmon resonances, but also an absorption flank at high photon energies, that cannot be seen in the calculations. It is assumed that the flank is to be ascribed to a mixture of $ZrN_{1-x}O_x$ particles, that formed due to the residual oxygen in the high-purity seeding gas. Their extinction spectrum shows an oxygen content dependent, monotone increase always starting at $\hbar\omega \approx 1$–2 eV. Provided that the condition

$$E = E_{\mathrm{ZrN}} + E_{\mathrm{ZrN}_{1-x}\mathrm{O}_x}$$

can be applied, the zirconium oxynitride particles add a monotone background increasing towards the UV to the ZrN spectrum. Comparing the shape of the flanks with classical Mie theory calculations of $ZrN_{1-x}O_x$-nanoparticles (Fig. 9), it was possible to specify a range for the oxygen content x, that may play a role: $0.2 < x < 0.5$.

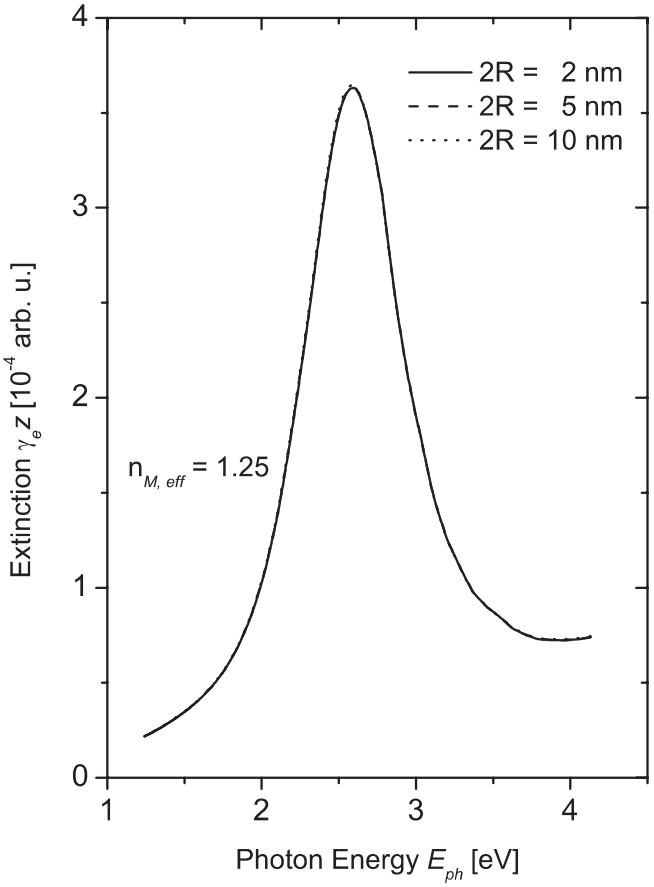

FIGURE 7 Classical Mie theory [2] calculations for the extinction of monodisperse spherical ZrN nanoparticles with a diameter of $2R = 2.0$, 5.0, and 10.0 nm. They were embedded into an artificial matrix material with $n_{\mathrm{M,eff}} = 1.25$, respecting the influence of the substrate on the optical spectrum [9]. The dielectric function of ZrN (for $T = 20\,^{\circ}\mathrm{C}$) was taken from [10]

Subtracting the extrapolated background given by the absorption flanks, the peak positions and the widths of the experimental data were determined (Table 3). As can be clearly seen from the data, all values for $\hbar\omega_{\mathrm{max}}$ are red shifted by $\Delta\hbar\omega = 0.7 \pm 0.1$ eV against the predicted peak position and stay fixed at $\hbar\omega_{\mathrm{max}} = 1.9$ eV within the margin of error. Γ, however, increases with the particle size/the seeding gas flow. Since Γ is sensitive to the extrapolation conditions, the values in Table 3 are rough estimates, only, and a considerable systematic error is present.

The deviations from the calculations can be explained as follows. On the one hand, four facts were not taken into account for this first computation of the Mie spectra:

Firstly, the nanoparticles are not perfectly spherical as discussed in Sect. 3.1. According to Hövel et al. [8] and

Sample	$\hbar\omega_{\mathrm{max}}$ [eV]	Γ [eV]
1	1.8 ± 0.1	1.2
2	2.0 ± 0.1	1.6
3	1.8 ± 0.1	2.0

TABLE 3 Peak positions and widths of the investigated samples. Both values were determined for each sample by subtracting an extrapolated monotone background, which is given by the respective absorption flank increasing towards the near UV (see Fig. 8)

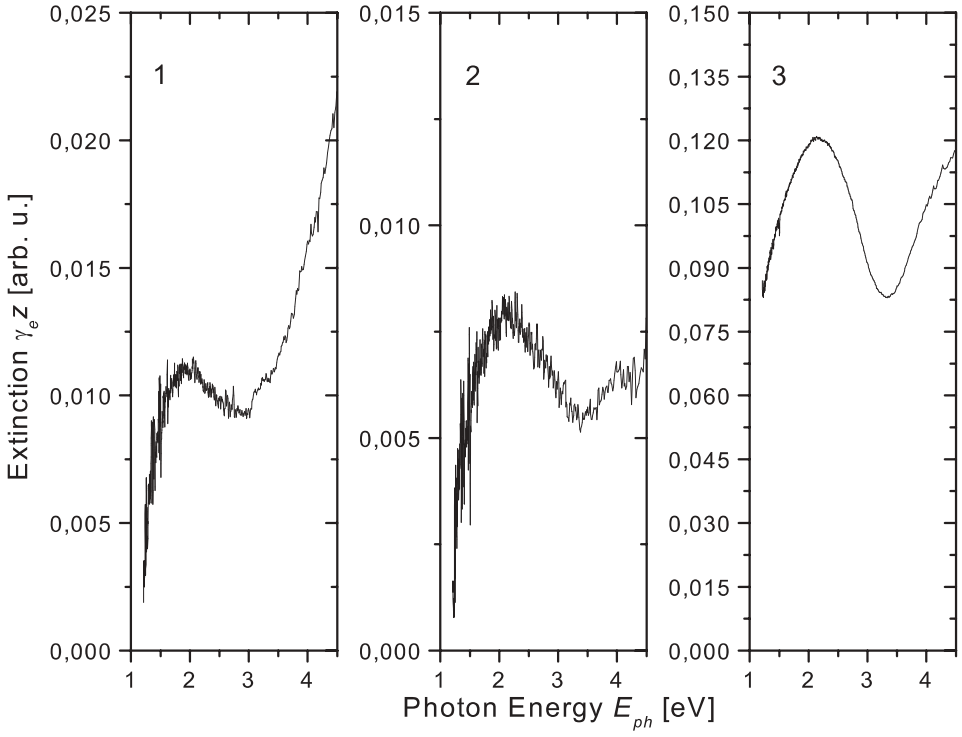

FIGURE 8 Optical extinction spectra calculated from the in-situ transmission spectra (see text). The average size of the particles is (1) 5.5 nm, (2) 6.0 nm, and (3) 6.5 nm, respectively. Note the different scales of the ordinates

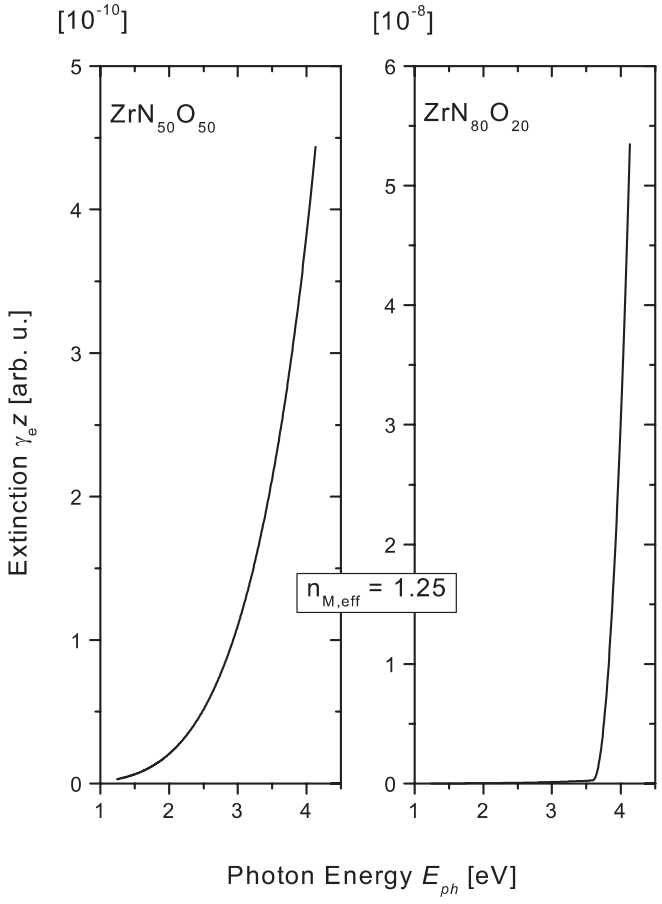

FIGURE 9 Classical Mie theory calculations for the extinction of monodisperse spherical $ZrN_{1-x}O_x$ nanoparticles with a diameter of $\langle 2R\rangle = 5$ nm. The surrounding material was modelled by the artificial matrix material with $n_{M,\mathrm{eff}} = 1.25$ (see text). The dielectric functions of the zirconium oxynitrides were taken from [11]. Note, that the extinction decreases strongly with increasing oxygen content x. Thus, the ordinates have different scales

Hilger et al. [9], the deviation from the perfectly spherical shape affects the spectrum in the way that the plasmon resonance maximum shifts towards lower energies.

Secondly, the Mie resonances in particle aggregate systems are coupled by electromagnetic stray fields, yielding peak shifts, peak splitting and broadening [2].

Thirdly, the electron wavefunctions of nanoparticles in coalescence aggregates interact with each other. This can lead to additional red shifts and to broadening of the resonance width [2, 8].

Fourthly, particle size dependencies of the dielectric function of the particle material [2] should also cause broadening and red shift of the plasmon resonance.

On the other hand, the residual oxygen certainly affects the deposited particles. It is expected that oxygen enters the particles and a shell of $ZrN_{1-x}O_x$ is formed. For shells with an oxygen contents of $x = 0.5$, Fig. 10 shows the calculations with the extended core-shell Mie theory [2].

The graphs indicate a shift of the resonance maximum towards lower energies with increasing shell thickness. The biggest change in the spectrum already occurs with thicknesses smaller than 1 nm. Further thickness increases leads to small additional changes only. The resonance maximum approaches $\hbar\omega_{\max}^{\mathrm{calc,cs}} \approx 1.8$ eV for shell thicknesses above 2 nm, which denotes a maximum shift of $\Delta\hbar\omega \approx 0.8$ eV compared to the pure ZrN particle.

As one can clearly see, this formation of oxynitride describes the deviations between the experimental data and the initial calculations very well. It is believed that this is the main reason for the observed peak shift. But since the alternative reasons, mentioned above for a peak shift, have also to be taken into account, the thickness of the shells cannot be determined by simply comparing experimental data and calculations.

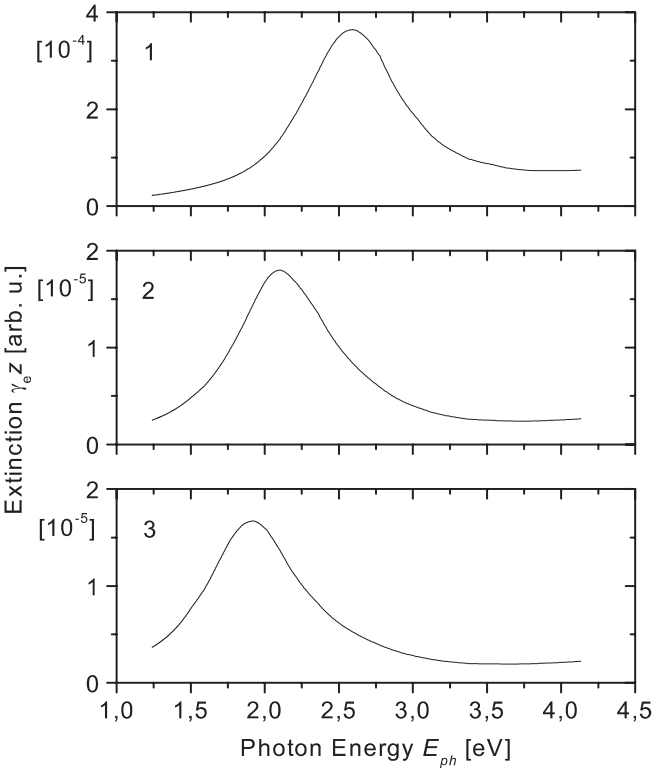

FIGURE 10 Mie calculations for $ZrN/ZrN_{0.5}O_{0.5}$ core-shell particles with $R = 3$ nm embedded in a matrix material with an effective refractive index of $n_{M,eff} = 1.25$. From *top* to *bottom* the core and the shell radii are: (1) 3 nm/0 nm, (2) 2 nm/1 nm, and (3) 1 nm/2 nm. Note the different scales of the ordinates

4 Summary

This work demonstrated the production of ZrN nanoparticles by laser ablation/evaporation with the LUCAS source. Particles of different mean sizes and fairly narrow size distributions were prepared with different N_2-seeding gas flows.

The SIMS analysis of a densely packed cluster film revealed, that their composition is almost stoichiometric ($Zr_{43}N_{57}$).

The ring pattern analysis of the TEM diffraction showed, that the nanoparticles mainly consist of a fcc structure (ZrN, ZrO). A tetragonal lattice component was also found and was ascribed to ZrO_2.

Optical spectroscopy measurements were carried out in-situ, indicating one single plasmon resonance in the visible. Classical Mie theory calculations suggest that the resonance shape and position only weakly depend on the particle size and that the peak should appear at $\hbar\omega_{max}^{calc} \approx 2.6$ eV with a width of $\Gamma^{calc} \approx 0.83$ eV for the examined single particles. The experimentally determined resonances of the many-particle systems, however, were red shifted by $\Delta\hbar\omega = 0.7 \pm 0.1$ eV compared to this value, and were additionally broadened.

It was shown by Mie calculations extended to core-shell particles [2], that an oxynitride shell is mainly responsible for these deviations. Already small shells shift the resonance maximum for several tenths of an electron volt towards lower energies. Taking into account also that particle-particle interactions, particle deformation, and aggregation are present in the samples and lead to red shifts too, it was not possible to determine the shell thickness by comparing the experimental data and the calculations. However, this can be done by high resolution TEM analysis.

ACKNOWLEDGEMENTS We are grateful to the Deutsche Forschungsgemeinschaft for the financial support of A. Reinholdt (Project KR 637/15) and the Alexander von Humboldt Foundation for the support of Dr. A. L. Stepanov.

We would also like to thank J. Ngaruiya for the preparation of the magnetron sputtered ZrN reference sample used in the SIMS analysis.

REFERENCES

1 D. Wu, Z. Zhang, W. Fu, X. Fan, H. Guo: Appl. Phys. A **64**, 593-595 (1997)
2 U. Kreibig, M. Vollmer: *Optical Properties of Metal Clusters* (Springer-Verlag, Berlin, Heidelberg 1995)
3 A.L. Stepanov, M. Gartz, G. Bour, A. Reinholdt, U. Kreibig: Vacuum **67**, 223-227 (2002)
4 M. Gartz: *Clusterphysik mit LUCAS, einer neuartigen Laser-Nanoteilchen-Quelle höchster Leistung* (Aachener Beiträge zur Physik der kondensierten Materie Bd. 31, Wissenschaftsverlag Mainz, Aachen 2001)
5 H. Spillmann, P.R. Willmott, M. Morstein, P.J. Uggowitzer: Appl. Phys. A **73**, 441 (2001)
6 W. Bieck, H. Gnaser, H. Oechsner: J. Vac. Sci. Technol. A.,**12**, 2537 (1994)
7 H.C. van de Hulst: *Light Scattering by Small Particles* (Dover Inc., NY 1981)
8 H. Hövel, A. Hilger, I. Nusch, U. Kreibig: Z. Phys. D **42**, 203 (1997)
9 A. Hilger, M. Tenfelde, U. Kreibig: Appl. Phys. B **73**, 361 (2001)
10 J.C. François, J. Casset, G. Chassaing, P. Gravier, and M. Sigrist: J. Appl. Phys. **58** (10), 3841 (1985)
11 S. Venkataraj, O. Kappertz, R, Jayavel, M. Wuttig: J. Appl. Phys. **92** (5), 2461 (2002)